

# Efficacy of a novel three-step decontamination protocol for titanium-based dental implants: An in vitro and in vivo study

Raphael Cavalcante Costa<sup>1</sup> | Thais Terumi Sadamitsu Takeda<sup>1</sup>  | Caroline Dini<sup>1</sup> |  
 Martinna Bertolini<sup>2</sup>  | Raquel Carla Ferreira<sup>3</sup> | Gabriele Pereira<sup>3</sup> |  
 Catharina Marques Sacramento<sup>1</sup> | Karina Gonzales S. Ruiz<sup>1</sup> | Magda Feres<sup>3,4</sup> |  
 Jamil A. Shibli<sup>3</sup>  | Valentim A. R. Barão<sup>1</sup>  | João Gabriel S. Souza<sup>3</sup> 

<sup>1</sup>Department of Prosthodontics and Periodontology, Piracicaba Dental School, University of Campinas (UNICAMP), Piracicaba, São Paulo, Brazil

<sup>2</sup>Department of Periodontics and Preventive Dentistry, School of Dental Medicine, University of Pittsburgh, Pittsburgh, Pennsylvania, USA

<sup>3</sup>Department of Periodontology, Dental Research Division, Guarulhos University, Guarulhos, São Paulo, Brazil

<sup>4</sup>Department of Oral Medicine, Infection and Immunity, Harvard School of Dental Medicine, Boston, Massachusetts, USA

## Correspondence

Valentim A. R. Barão, University of Campinas (UNICAMP), Piracicaba Dental School, Department of Prosthodontics and Periodontology, Av. Limeira, 901, Piracicaba, São Paulo 13414-903, Brazil.  
 Email: [vbarao@unicamp.br](mailto:vbarao@unicamp.br)

João Gabriel S. Souza, Department of Periodontology, Dental Research Division, Guarulhos University, Guarulhos, São Paulo 07023-070, Brazil.  
 Email: [jgabriel.souza@yahoo.com.br](mailto:jgabriel.souza@yahoo.com.br)

## Funding information

Conselho Nacional de Desenvolvimento Científico e Tecnológico; Coordenação de Aperfeiçoamento de Pessoal de Nível Superior; Fundação de Amparo à Pesquisa do Estado de São Paulo

## Abstract

**Aim:** The aim of the study was to evaluate several mechanical and chemical decontamination methods associated with a newly introduced biofilm matrix disruption strategy for biofilm cleaning and preservation of implant surface features.

**Materials and Methods:** Titanium (Ti) discs were obtained by additive manufacturing. Polymicrobial biofilm-covered Ti disc surfaces were decontaminated with mechanical [Ti curette, Teflon curette, Ti brush, water-air jet device, and Er:YAG laser] or chemical [iodopovidone (PVPI) 0.2% to disrupt the extracellular matrix, along with amoxicillin; minocycline; tetracycline; H<sub>2</sub>O<sub>2</sub> 3%; chlorhexidine 0.2%; NaOCl 0.95%; hydrocarbon-oxo-borate-based antiseptic] protocols. The optimal in vitro mechanical/chemical protocol was then tested in combination using an in vivo biofilm model with intra-oral devices.

**Results:** Er:YAG laser treatment displayed optimum surface cleaning by biofilm removal with minimal deleterious damage to the surface, smaller Ti release, good corrosion stability, and improved fibroblast readhesion. NaOCl 0.95% was the most promising agent to reduce in vitro and in vivo biofilms and was even more effective when associated with PVPI 0.2% as a pre-treatment to disrupt the biofilm matrix. The combination of Er:YAG laser followed by PVPI 0.2% plus NaOCl 0.95% promoted efficient decontamination of rough Ti surfaces by disrupting the biofilm matrix and killing remnants of in vivo biofilms formed in the mouth (the only protocol to lead to ~99% biofilm eradication).

**Conclusion:** Er:YAG laser + PVPI 0.2% + NaOCl 0.95% can be a reliable decontamination protocol for Ti surfaces, eliminating microbial biofilms without damaging the implant surface.

## KEYWORDS

decontamination, Dental implant, Biofilm, Peri-implantitis

Raphael Cavalcante Costa and Thais Terumi Sadamitsu Takeda share the position of first authors.

Valentim A. R. Barão and João Gabriel S. Souza share the position of senior authors.

© 2023 John Wiley & Sons A/S. Published by John Wiley & Sons Ltd.

## 1 | INTRODUCTION

Dental implants are a reliable and predictable treatment option for supporting dental prostheses with high clinical longevity and survival rates (Howe et al., 2019). However, immune-mediated biological complications attributed to polymicrobial biofilms formed around the implant often lead to peri-implant diseases, such as peri-implant mucositis and peri-implantitis (Berglundh et al., 2018). Once the biofilm accumulates on the irregular topography of implant surfaces, treatments involving effective microbial removal become very challenging for clinicians due to the complex biofilm architecture, which is highly specialized to favor coaggregation and cell protection through the extracellular biofilm matrix (Costa, Souza, Bertolini, et al., 2020; Costa, Souza, Cordeiro, et al., 2020; Yang et al., 2023). Meta-analyses have shown that peri-implantitis can affect 12%–24% of patients 5–10 years after implant placement (Derks & Tomasi, 2015; Lee et al., 2017). Furthermore, peri-implant diseases continue to rise worldwide due to the popularity of dental implants and population aging and are considered an emergent global public health problem (Costa, Abdo, et al., 2021; Costa, Nagay, et al., 2021). Therefore, since pathogenic biofilm accumulation on implant material is a major cause of peri-implant diseases, surface decontamination is a prerequisite to successful therapy for implant-related diseases (Cosgarea et al., 2022).

Implant decontamination can be performed with nonsurgical and surgical interventions using a plethora of physical and chemical protocols (Louropoulou et al., 2014; Ntrouka et al., 2011). Regarding nonsurgical therapies, conventional mechanical debridement with various types of scalers, ultrasonic tips, brushes, or alternative approaches such as oral irrigators, air-abrasive devices, and laser therapies are commonly used to clean contaminated implants (Cosgarea et al., 2022; Figuero et al., 2014). Nevertheless, these mechanical therapies have shortcomings due to their limited accessibility for cleaning the complex rough titanium (Ti) implant surface, hindering effective biofilm removal (Costa, Souza, Bertolini, et al., 2020; Costa, Souza, Cordeiro, et al., 2020). If the remaining biofilm structure is not removed, it may promote microbial recolonization and persistent infection (Bowen et al., 2018). For this reason, chemotherapeutic agents have also been applied as an adjunct to subgingival instrumentation (Balderrama et al., 2020). However, the effectiveness of disinfection protocols remains unpredictable and reported beneficial clinical outcomes might be restricted to a short-term period, especially if implant surfaces are left exposed in the oral cavity (Renvert et al., 2008; Shibli et al., 2019). Currently, no particular treatment is considered the gold standard for disrupting the biofilm matrix and efficiently reducing the bacterial load below the threshold level for predictable nonsurgical treatment outcomes, raising the need for biofilm-focused treatment modalities (Cosgarea et al., 2022; Figuero et al., 2014; Heitz-Mayfield & Mombelli, 2014). In this context, strategies for disrupting bacterial clustering and the exopolysaccharide matrix to enhance biofilm removal have been suggested to overcome the therapeutic limitation of peri-implantitis treatment, but this novel strategy is still being underutilized (Costa et al., 2022; Souza et al., 2022; Yang et al., 2023).

The 2017 World Workshop on the Classification of Periodontal and Peri-Implant Diseases and Conditions consensus report recognized that an optimal decontamination protocol should ensure both cleaning potential by biofilm removal and maintenance of implant surface features to possibly achieve the biological seal of the implant-soft tissue interface and re-osseointegration afterward (Berglundh et al., 2018). However, this protocol has not yet been established. This goal becomes a particular challenge with the rough Ti surfaces currently used in dental implants compared with the classic turned implants initially used by Branemark (Howe et al., 2019). Here, we conducted *in vitro* and *in vivo* studies aiming to examine not only Ti surface decontamination efficacy but also their possible deleterious effects on a 3D-printed rough surface, including Ti release, corrosion behavior, and posterior fibroblast cytocompatibility. Collectively, we unveil a promising combined mechanical/chemical protocol based on the initial biofilm matrix disruption strategy associated with bacterial killing and removal to effectively decontaminate complex rough dental implant surfaces.

## 2 | MATERIALS AND METHODS

### 2.1 | Experimental design and ethical aspects

This study was designed with emerging mechanical and chemical protocols for dental implant decontamination currently used in the clinic setting (Figure S1). Importantly, a matrix-degrading agent was used prior to chemical therapy to further enhance bacterial killing on the implant surface. In brief, *in vitro* tests were conducted to evaluate the best treatment for promoting minimum surface damage without altering the posterior fibroblasts adhesion, morphology, and spreading. Additionally, polymicrobial biofilm-covered surfaces were also tested to confirm efficient biofilm removal and bacteria viability using mechanical and chemical protocols. Next, chemotherapeutic agents were tested in combination with a pre-treatment with PVPI 0.2% to determine the best *in vitro* surface disinfection. Last, the best mechanical/chemical protocol, optimized by PVPI 0.2% application, was evaluated against biofilms formed in the oral environment using our validated *in vivo* model for implant surfaces with palatal appliances in healthy volunteers (Souza, Cury, et al., 2019) to determine the efficiency of the established three-step decontamination protocol. This study was approved by the Local Research and Ethics Committee (protocol 53844321.2.0000.5418) and was conducted in according to Brazilian ethical regulations (National Health Council, resolution 466/12) and the Declaration of Helsinki.

### 2.2 | Rough Ti implant surfaces

Rough Ti surface discs (Ø12 mm x 2 mm) were made of Ti-6Al-4V powders with a particle size of 25–45 µm by additive manufacturing technology (Pinguero et al., 2019). The titanium discs presented a hierarchical surface referent to the commercial Plenum® implant

surface (Jundiaí, São Paulo, Brazil). The selection of this implant surface was based on the difficulty to remove bacteria from the highly rougher surfaces (Ra value: 7.70  $\mu\text{m}$ ), thus being a relevant condition to determine the best effect of decontamination protocols.

### 2.3 | Mechanical instrumentation protocols

A calibration process was performed prior to the commencement of the study to ensure the reproducibility of the decontamination methods. Two examiners (R.C.C. and T.T.S.T.) were calibrated by calculating the intraclass correlation coefficient (ICC = 0.834;  $p < .0001$ ; two-way random-effects model) based on the load applied ( $N$ ) in hand instruments during the decontamination of implant surfaces on two separate occasions, 1 week apart. The ICC was adopted as a measure to promote/calibrate mechanical instrumentations with reliability across all experimental method (decontamination without and with biofilm on the surface). After a pilot study, each sample was instrumented for 60s utilizing a sterile technique. The discs were randomly and equally allocated to the following decontamination protocols:

1. *As-received*: control group without instrumentation.
2. *Titanium curette* (M. Polachini, São Paulo, SP, Brazil): Manually treated with a working force of  $\sim 0.25\text{ N}$  and an angle of  $70\text{--}80^\circ$ , moving in an imbricate style with 20 strokes, and immersed in deionized water.
3. *Teflon curette* (M. Polachini, São Paulo, SP, Brazil): Manually treated with a working force of  $\sim 0.25\text{ N}$  and an angle of  $70\text{--}80^\circ$ , moving in an imbricate style with 20 strokes, and immersed in deionized water.
4. *Titanium brush* (Salvin Dental, Charlotte, NC, USA): Rotatory brushes were coupled in the oscillating dental handpiece at 600rpm, with irrigation of deionized water, light pressure, and at an angle of approximately  $45\text{--}60^\circ$  as recommended in the instructions for use by the manufacturer for nonflap cases.
5. *Water-air jet* (Oraljet, Campinas, SP, Brazil): A standard handpiece was mounted with a holder to maintain the nozzle at a static position, perpendicular to the disc, to treat each sample at a distance of 10mm with a static pressure of 7bar (101.5psi) and 60mL of deionized water/min.
6. *Erbium-doped yttrium aluminum garnet (Er:YAG) laser* (Life touch®, Light Instruments, São Paulo, SP, Brazil): laser irradiation with the tip  $1.3 \times 17\text{ mm}$ , perpendicular to the disc, at a distance of 10mm with laser beam parameters using the manufacturers' recommended setting for implant recovery (40mJ, 0.80W, 20Hz, in continuous mode).

To simulate clinical practice, the force exerted in hand instruments (protocols 2 and 3) is consistent with those that would be used to remove adherent calculus deposits from implant surfaces (Lang et al., 2016). For the automatic tools (protocols 4, 5, and 6), each disc received treatment by being consistently rotated opposing the nozzle from the center to the periphery in 10 circular motions.

After instrumentation, all the discs were cleaned with deionized water. These mechanical instrumentations were performed in the presence and absence of oral biofilms.

### 2.4 | Chemical decontamination protocols

Biofilm-covered implant surfaces were randomly and equally allocated to treated by immersion in a 24-well plate with 1mL (v/v) of seven different chemotherapeutic agents and incubated under static conditions ( $\pm 37^\circ\text{C}$ ; 10%  $\text{CO}_2$ ) for 10min, as follows:

1. *Sterile saline* [NaCl; 0.9%–v/v]: control group without disinfection treatment.
2. *Amoxicillin* [AMX; 4.14  $\mu\text{g}/\text{mL}$ ] (Sigma–Aldrich, St. Louis, MO, USA) to simulate the concentrations detected in the pocket environment following systemic administration (Tenenbaum et al., 1997).
3. *Minocycline* [MIN; 1.49  $\mu\text{g}/\text{mL}$ ] (Sigma–Aldrich, St. Louis, MO, USA) to simulate the concentrations detected in the pocket environment following systemic administration (Sakellari et al., 2000).
4. *Tetracycline* [TEC; 0.61  $\mu\text{g}/\text{mL}$ ] (Sigma–Aldrich, St. Louis, MO, USA) to simulate the concentrations detected in the pocket environment following systemic administration (Sakellari et al., 2000).
5. *Hydrogen peroxide* [ $\text{H}_2\text{O}_2$ ; 3%–v/v] (Sigma–Aldrich, St. Louis, MO, USA) to mimic the local irrigation performed by professionals during clinical practice (Jervøe-Storm et al., 2021).
6. *Chlorhexidine* [CHX; 0.2%–v/v] (Sigma–Aldrich, St. Louis, MO, USA) to mimic the local irrigation performed by professionals during clinical practice (Souza et al., 2018).
7. *Hydrocarbon-oxo-borate-based formula antiseptic* [HCOBc; 1mL –v/v] (BlueM®, Curitiba, PR, Brazil): To mimic the mouthwashes performed by patients in the oral care routine (Shibli et al., 2021).
8. *Sodium hypochlorite* [NaOCl; 0.95%–v/v] (Sigma–Aldrich, St. Louis, MO, USA) to mimic local administration by professionals during clinical practice (Radulescu et al., 2022). After each treatment, samples were washed in 0.9% NaCl solution, and biofilm analysis was immediately conducted.

### 2.5 | Biofilm matrix-degrading therapy

Biofilm matrix-targeting therapy using PVPI 2% (v/v) to disrupt extracellular matrix compounds was previously tested on smooth Ti surfaces by our group (Costa, Souza, Bertolini, et al., 2020; Costa, Souza, Cordeiro, et al., 2020). We are now in a position to deepen and improve the method to completely clean contaminated implant surfaces, including highly rough Ti implant surfaces. As a proof-of-concept analysis, an in vitro dose–response assay was conducted to determine the minimum therapeutic concentration of PVPI and the amounts of soluble extracellular polysaccharides and insoluble extracellular polysaccharides after PVPI treatment (Please see Figure S5). Based on these results, it was possible to determine the concentration and time of topical application (PVPI

## Mechanical protocols

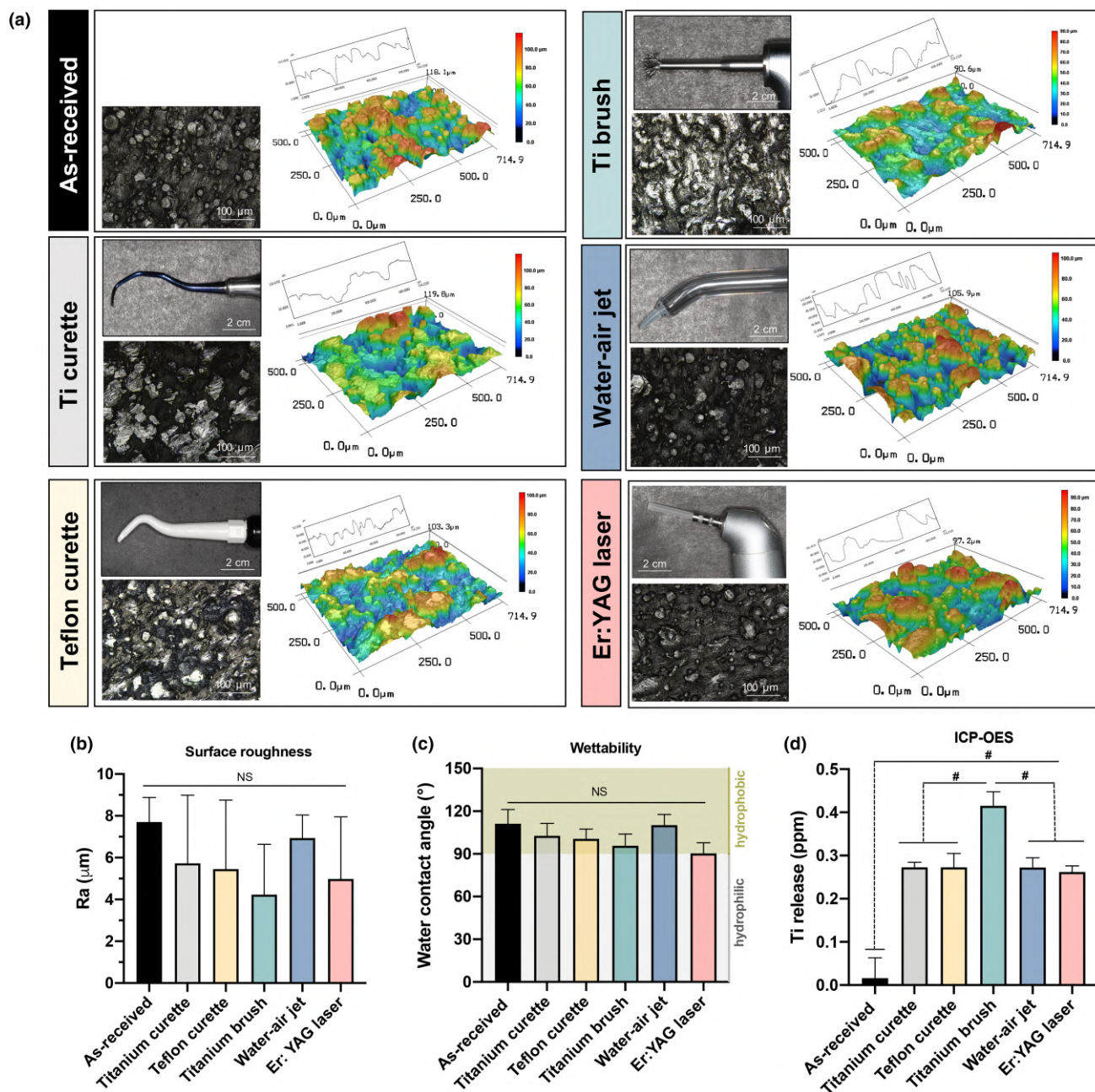


**FIGURE 1** Mechanical instrumentation protocols on 3D-printed implant surfaces. (a) Photographic images of each mechanical instrument (top panel, on the left); representative two- (bottom panel, on the left) and three- (bottom panel, on the right) dimensional images, and roughness profile (top panel, right) from each group ( $n=2$ ) obtained by confocal laser scanning microscopy (CLSM; 150 $\times$  magnification). (b) Roughness average (Ra) obtained by profilometry after mechanical instrumentation ( $n=6$ ). (c) Water contact angle after mechanical instrumentation ( $n=5$ ). Different background colors for the graph indicate the hydrophilicity scale. (d) Ti ion release was measured by inductively coupled plasma-optical emission spectrometry (ICP-OES) after mechanical instrumentation ( $n=3$ ). Data are expressed as the mean  $\pm$  standard deviation. Statistically significant differences between groups are indicated by symbols: # $p < 0.05$ , Tukey's HSD test. NS=no statistically significant differences.

0.2% [v/v] for 10min). The PVPI 0.2% biofilm matrix-degrading therapy was tested in vitro in combination with the best chemical protocols to evaluate the boost effect on bacterial killing. Then, PVPI 0.2% combined with the best chemical and mechanical protocol was tested in vivo.

## 2.6 | In vitro measure outcomes

The measure outcomes were implant surfaces features (topography, roughness parameters, wettability, and Ti ion release), corrosion performance, human gingival fibroblasts cell behavior (metabolism and

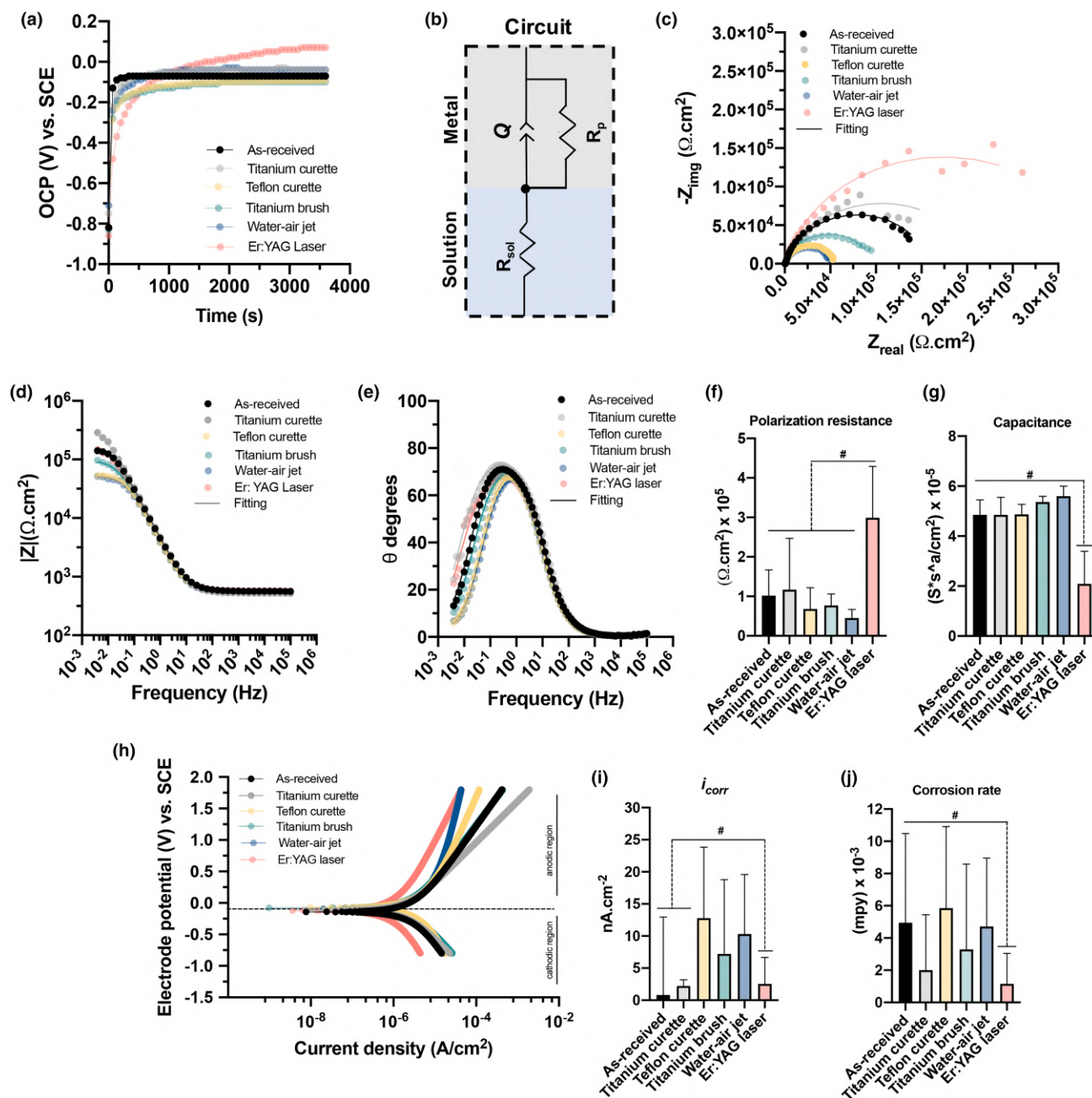


**FIGURE 2** Corrosion performance of titanium implant surface in artificial saliva as a function of different mechanical instrumentation ( $n=5$ ). (a) Representative curve of open circuit potential (OCP) evolution (in V vs. SCE – saturated calomel electrode) for 3600s. (b) The equivalent electric circuit used for electrochemical impedance spectroscopy (EIS) data, in which  $R_{sol}$  represents the resistance of the electrolyte,  $R_p$  is the polarization resistance, and  $Q$  is the constant phase element. Representative (c) Nyquist diagrams, (d) impedance modulus, and (e) phase angles of EIS. Electrical parameter values such as (f) polarization resistance and (g) capacitance are obtained from EIS (goodness of fit on the order of  $10^{-3}$ ). (h) Potentiodynamic polarization curves (in V vs. SCE). (i) Corrosion current density ( $i_{corr}$ ) and (j) corrosion rate values. Data are expressed as the mean  $\pm$  SD. Statistically significant differences between groups are indicated by symbols: # $p < .05$ , Tukey's HSD test.

morphology), and biofilm cleaning potential (microbial load and biofilm composition). Additional methodological details are in the Appendix S1.

## 2.7 | In vivo measure outcomes

The optimal mechanical/chemical protocol was tested in combination with PVPI treatment using an in vivo model for biofilm

formation. The protocol includes 3 steps as follows: (i) mechanical debridement; (ii) biofilm matrix-degrading therapy with PVPI (10 min); (iii) adjuvant chemical administration (10 min). For this, four healthy volunteers wore a palatal appliance containing Ti discs for 3 days, as described elsewhere (Souza, Cury, et al., 2019; Costa, Souza, Bertolini, et al., 2020; Costa, Souza, Cordeiro, et al., 2020). Samples ( $n=6$  per group) were exposed extraorally, four times/per day, to 20% (v/v) sucrose solution to allow the increase of

peri-implant associated pathogens with bacterial loads similar to that found on peri-implantitis (Souza, Cordeiro, et al., 2019; Souza, Cury, et al., 2019). On the morning of the fourth day, discs were removed, randomized, and treated by the established mechanical/chemical protocol. Untreated biofilms were used as controls. The antimicrobial efficacy was determined by CFU counts and reported as % of bacterial count reduction after treatment vs. control. After decontamination, the biofilm remnants were fully collected and inserted into a tube (weight verified previously), and then the tube containing the sample was weighed to estimate the biofilm wet weight (in mg) as an indicator of residual biomass (Souza, Cordeiro, et al., 2019; Souza, Cury, et al., 2019).

## 2.8 | Statistical analysis

GraphPad Prism software (GraphPad, La Jolla, CA, USA) was used for statistical analyses and to prepare the final graphs. The normality of errors and homoscedasticity of data were checked for each response variable, considering each sample as a statistical unit. Data normality was checked using Shapiro–Wilk test. The quantitative data were subjected to analysis of variance (one-way ANOVA) in Tukey's HSD test for multiple comparisons. A significance level of 5% was considered to be statistically significant. The statistical power test was conducted using the G\*power software version 3.1.9.2 (Program written, conceptualized, and designed by Franz, Universitat Kiel, Germany). For this purpose, a priori two-tailed *t*-test to compute required sample size was run based on the mean and SD values for the in vitro CFU counts (Souza et al., 2022) (control vs. CHX treatment) and in situ CFU counts (Souza, Cordeiro, et al., 2019) (control–NaCl vs. Citric acid 40% immersion). A large size effect ( $1-\beta$  err prob=0.8, according to Cohen effect size statistics) and an  $\alpha$  err prob of 0.05 was considered. A total of four samples per group was required, generating an actual power of 0.83 and 0.84 for the in vitro and in vivo data, respectively. The entire dataset is available in a spreadsheet format and registered in a web-based institutional repository from the University of Campinas (UNICAMP).

## 3 | RESULTS

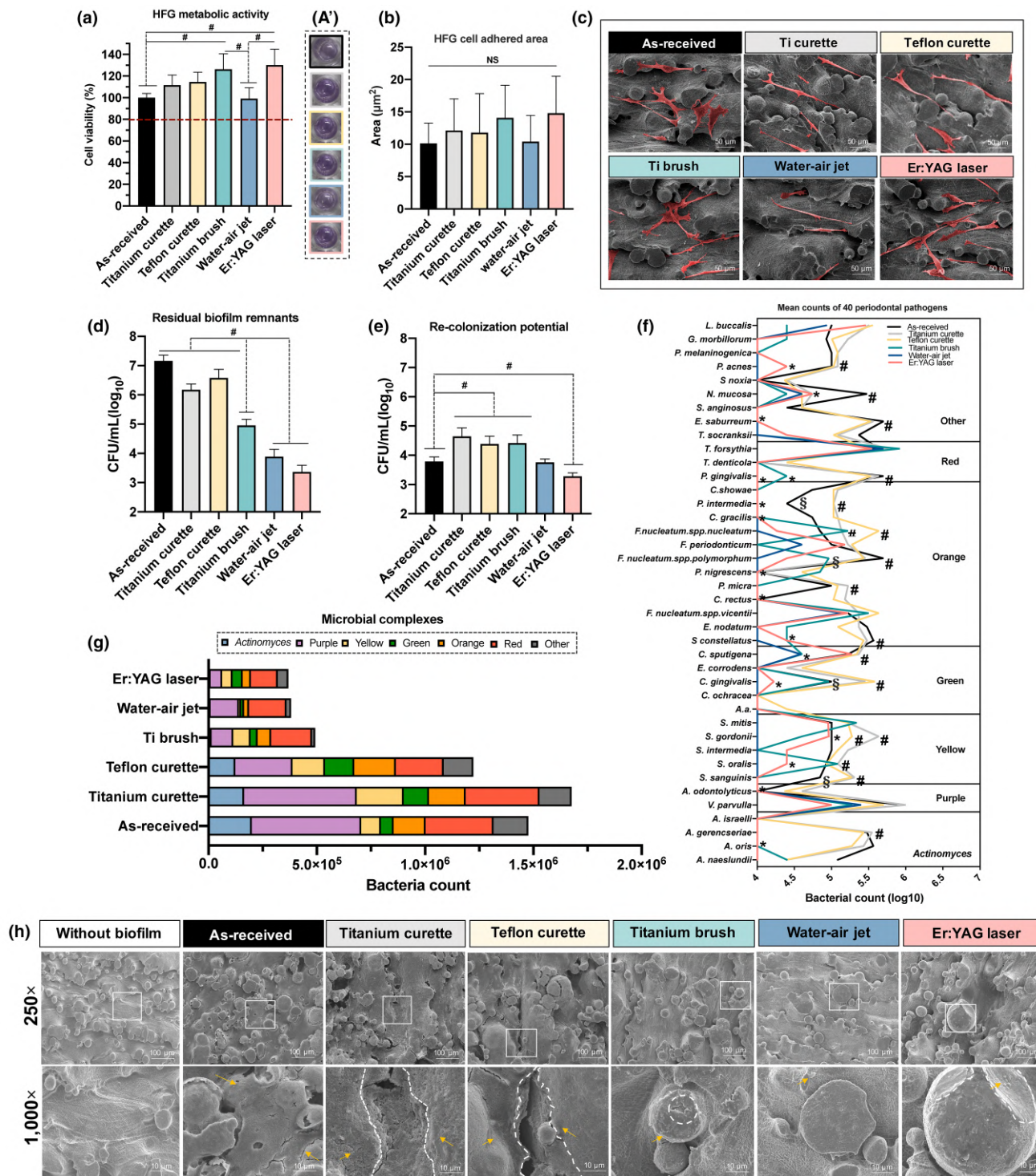
### 3.1 | Implant surface degradation

Two- and three-dimensional confocal images showed distinct effects on both the macro- and microstructure of the implant surface, leading to different roughness profiles for each treatment (Figure 1a). Mechanical instrumentation using a titanium brush, titanium curette, and Teflon curette generated significant surface damage and flattening peaks, leading to greater vertical discrepancies. The Er:YAG laser group showed an overall polished appearance with reduced sharpness of the peaks, while the valley area appeared unaffected. Finally, the water–air jet group showed no evident surface alterations. The two-dimensional average surface roughness values (Ra) of the as-received surface ( $7.70 \pm 1.18 \mu\text{m}$ ) remained unchanged even after each method of instrumentation ( $p > .05$ ; Figure 1b). Meanwhile, Rq, Rt, and Rz showed decreased values after Teflon curette instrumentations ( $p < .05$ ; Figure S2), probably due to the presence of Teflon debris on the treated-implant surfaces. The wettability property for all surfaces remained stable when compared to the as-received group ( $p > .05$ ; Figure 1c), with similar average contact angles and a tendency for hydrophobicity (From as-received:  $111.24^\circ \pm 9.9$  up to Er:YAG:  $90.31^\circ \pm 7.5$ ). Regarding surface degradation, titanium brush instrumentation induced the greatest Ti ion release (~4-fold increases compared to as-received), and this concentration was statistically significant in all groups ( $p < .05$ ; Figure 1d). The other groups showed no statistical difference among them, except with the as-received control group ( $p < .05$ ).

### 3.2 | Corrosion performance

The open circuit potential (OCP) curves of the Er:YAG laser stabilized in nobler potentials with the most positive values (Figure 2a). The electrochemical impedance spectroscopy (EIS) data were modeled using a simple equivalent electrical circuit (Figure 2b). For the Er:YAG laser group, the semicircular diameter of the Nyquist arch was the

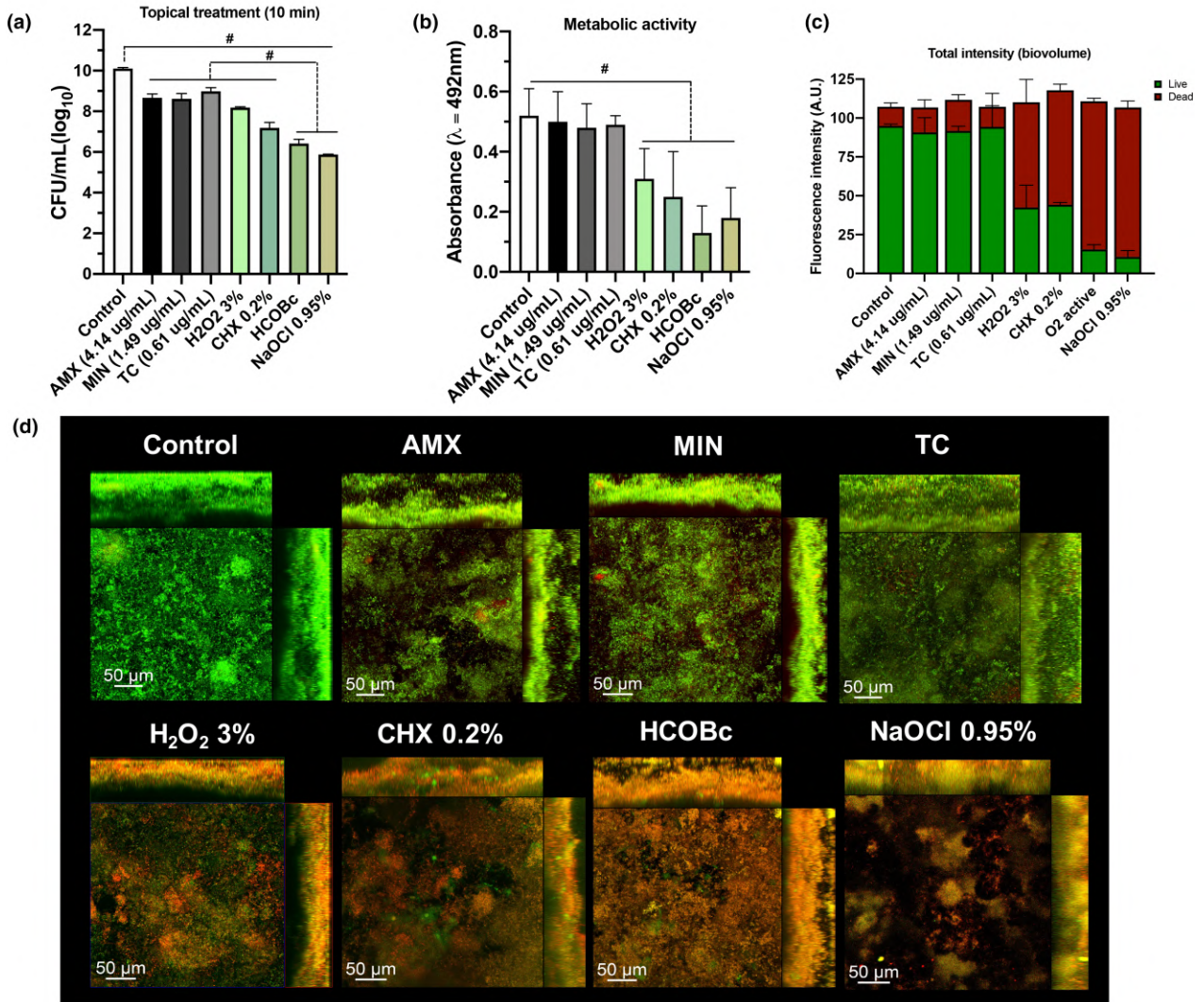
**FIGURE 3** In vitro cellular and microbiological results after mechanical instrumentation. (a) Human gingival fibroblast (HGF) metabolic activity (%) was evaluated by MTT assay after culturing in the mechanically treated surfaces from 1 day ( $n=6$ ) with (A) its photography of colorimetric changes in each group. (b) The HGF cell-adhered area ( $\mu\text{m}^2$ ) for each group was obtained from SEM micrographs (250 $\times$  magnification) and calculated using ImageJ software. HGF were colored in red using Adobe Photoshop CC 2018. (c) Representative SEM micrographs of HGF cell morphology and adhesion-treated surfaces after 1 day of cell culture (250 $\times$  magnification) using 15 kV. (d) Residual polymicrobial biofilm remnants formed in vitro (48 h) after mechanical decontamination reported as log-transformed viable colony-forming units (Log<sub>10</sub> CFU/mL) ( $n=6$ ). (e) The recolonization potential of treated surfaces after 1 h of bacterial adhesion reported as log-transformed viable colony-forming units (Log<sub>10</sub> CFU/mL) ( $n=6$ ). (f) Profile of mean levels of 40 bacterial species in biofilm samples (48 h) after mechanical instrumentation by checkerboard DNA–DNA hybridization ( $n=6$ ). Levels of individual species were computed in each sample and then averaged for each group. (g) Proportions of periodontal complexes using the mean of total levels of the species evaluated ( $n=6$ ). (h) SEM ( $n=2$ ) micrographs (magnification=250 $\times$  and 1000 $\times$ ) after mechanical instrumentation in polymicrobial biofilm (48 h) formed in vitro. The white lines represent the biofilm-removed areas and surface damage. Sterilized saline (0.9%) rinse was used as a control. Data are expressed as the mean  $\pm$  SD. Statistically significant differences between groups are indicated by symbols: # $p < .05$ , Tukey's HSD test. For checkerboard DNA–DNA hybridization analysis (f), symbol presence indicates a statistical difference ( $p < .05$ , Tukey's HSD test) of the group from the other ones (without symbol). Different symbols indicate statistical differences among the groups with symbols ( $p < .05$ , Tukey's HSD test). NS, no statistically significant differences.



widest, while in the Bode plot (Figure 2d) and phase angle (Figure 2e), the data remained rather stable throughout all groups at low frequencies. Polarization resistance ( $R_p$ ; Figure 2f), and capacitance ( $Q$ ; Figure 2g) showed excellent agreement between the experimental and simulated EIS data ( $\chi^2 \leq 10^{-3}$ ; Table S1). Notably, higher values of  $R_p$  ( $2.99 \pm 1.3 \Omega \text{cm}^2$ ) and smaller values of  $Q$  ( $2.09 \pm 1.3 \Omega^{-1} \text{s}^n \text{cm}^{-2}$ ) of the Ti oxide film can be seen for the Er:YAG group ( $p < .05$ ). For the potentiodynamic polarization (Figure 2h), the Er:YAG curves are

shifted to more electropositive potentials and slightly lower current densities than the as-received group. Regarding electrochemical parameters (Table S2), the Er:YAG laser exhibited significantly lower  $i_{\text{corr}}$  (Figure 2i;  $2.54 \pm 4.1 \mu\text{A cm}^{-2}$ ) and corrosion rate (Figure 2j;  $1.16 \pm 1.9 \text{mpy}$ ) than those of the as-received group. Altogether, the Er:YAG laser group exhibited slight improvement in some electrical and electrochemical parameters compared to the other groups. In addition to corrosion assessments, XPS analysis (Figure S3) revealed a

### Chemical protocols



### Biofilm matrix-targeting therapy

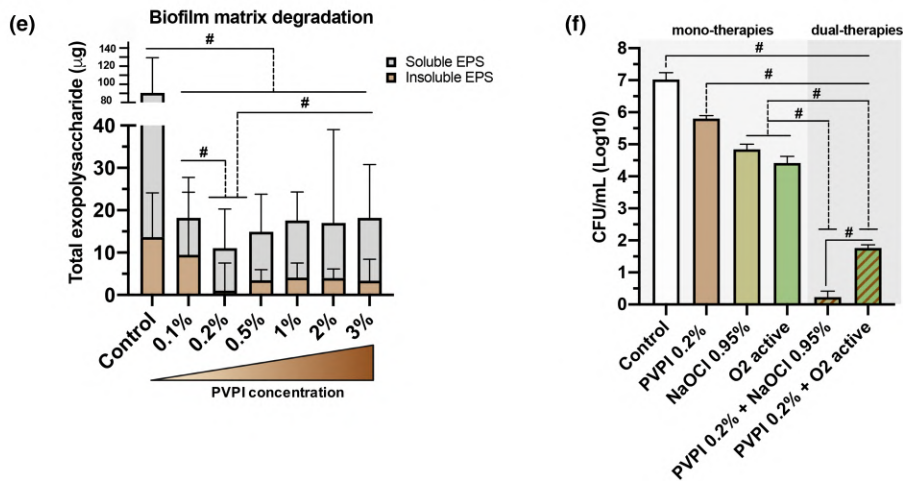


**FIGURE 4** Adjuvant chemical protocols and biofilm matrix-degrading therapy on 3D-printed implant surfaces. (a) Log-transformed viable colony-forming units (Log<sub>10</sub> CFU/mL) and (b) bacterial metabolic activity evaluated by XTT assay after topical chemical protocol applications (10 min) on 48-h biofilm formed in vitro ( $n=5$ ). (c) Average total fluorescence intensity (by area - 400  $\mu\text{m}^2$ ) of live and dead cells in A.U. (arbitrary units) from fluorescence images ( $n=2$ ). (d) Bacterial cell viability ( $n=3$ ) after chemical treatments via live/dead analysis (green for live cells, red for dead cells; R.O.I = 102.53  $\mu\text{m}^2$ ). (e) Dose-response assay quantified by the phenol sulfuric method to determine the amounts of soluble extracellular polysaccharides and insoluble extracellular polysaccharides ( $n=6$ ). Data are expressed in  $\mu\text{g}$  polysaccharides. (f) Log-transformed viable colony-forming units (Log<sub>10</sub> CFU/mL) after topical mono- and dual-therapy applications (10 min of each) on 48-h biofilm formed in vitro ( $n=5$ ). Different graph background colors show the type of therapy regarding the number of treatment immersions. Sterilized saline (0.9%) rinse was used as a control. Data are expressed as the mean  $\pm$  SD. Statistically significant differences between groups are indicated by symbols: # $p < .05$ , Tukey's HSD test. Abbreviations: AMX, amoxicillin; CHX, chlorhexidine; H<sub>2</sub>O<sub>2</sub>, hydrogen peroxide; HCOBc, hydrocarbon-oxo-borate; MIN, minocycline; NaOCl, sodium hypochlorite; TEC, tetracycline.

minimal impact of mechanical instrumentation on the chemical composition in the outermost oxide layer formed on the Ti substrates.

### 3.3 | Cell behavior and biofilm cleaning potential

An adequate cell-surface interaction was observed after all mechanical instrumentation modalities (Figure 3a,a'), evidencing greater fibroblasts metabolism in the titanium brush and Er:YAG laser groups (~20% increase vs. as-received group;  $p < .05$ ). However, no significant difference was found in the cell-adhered area ( $p > .05$ ; Figure 3b), which was around 10–20  $\mu\text{m}^2$  of cell coverage. SEM micrographs showed that fibroblasts were able to attach and spread on the treated surfaces with a preferred orientation in the valley area (Figure 3c). Regarding microbiological findings, none of the protocols promoted total polymicrobial biofilm eradication from rough Ti implant surfaces (Figure 3d). However, the water-air jet and Er:YAG laser successfully removed the majority of the bacteria (~4-log reduction, compared to the as-received group) (Figure S4A), resulting in a small load of residual biofilm remnants ( $p < .05$ ). The Er:YAG laser was the only mechanical protocol to slightly reduce bacterial recolonization after instrumentation ( $p < .05$ ; Figure 3e). The 40 bacterial species assessed were detected in all treatment groups (Figure 3f). Some periodontal pathogens such as *Treponema denticola*, *Porphyromonas gingivalis*, *Campylobacter showae*, *Prevotella intermedia*, *Campylobacter gracilis*, *Prevotella nigrescens*, *Parvimonas micra*, *Campylobacter rectus*, and *Eubacterium nodatum*, were reduced on the laser-treated surface (~1 log of DNA count reduction vs. as-received group;  $p < .05$ ), promoting the reduction of red and orange complexes load (Figure 3g). Therefore, Er:YAG laser led to biofilm removal and less virulent remnant biofilm. SEM micrographs (Figure 3h) indicated the presence of microbial clusters hiding in the pits and valleys from the implant surface. The titanium brush, water-air jet, and Er:YAG laser reached and dislodged the bacteria in these valley areas.

### 3.4 | Chemical decontamination and biofilm matrix-degrading therapy

Compared with saline rinsing (control), all chemical protocols significantly reduced the microbial viability, although with significant

differences among the treatment regimens (Figure 4a). The best antimicrobial protocol was found for NaOCl 0.95%, followed by HCOBc, with an almost 6-fold and 5-fold decrease in bacterial viability compared to the control, respectively (Figure S4B). The metabolic activity of biofilms exposed to NaOCl 0.95% and HCOBc also displayed the greatest reduction compared with the control ( $p < .05$ ; Figure 4b). These data were validated by fluorescence images (Figure 4c), in which polymicrobial biofilms were more susceptible to NaOCl 0.95% and HCOBc application with a higher proportion of dead cells (in red) among all groups. In fact, the total fluorescence intensity of dead bacterial cells was more pronounced in NaOCl 0.95% (Figure 4d). For matrix-targeted therapy (Figure 4e and Figure S5), 0.2% PVPI was the most effective for both soluble and insoluble exopolysaccharide matrix degradation ( $p < .05$ ). Therefore, PVPI 0.2% treatment before NaOCl and HCOBc antimicrobials was the standard protocol to demonstrate the proof-of-concept for this approach (Figure 4f). Although PVPI 0.2% is devoid of strong antimicrobial ability alone, when used as a pre-treatment, it significantly enhanced the antimicrobial activity of NaOCl 0.95% (~4.5-log more effective killing vs. antimicrobial alone;  $p < .05$ ). When comparing NaOCl and HCOBc, in the dual therapy, the PVPI + NaOCl combination was more effective than PVPI + HCOBc ( $p < .05$ ; Figure 4f).

### 3.5 | In vivo antimicrobial efficacy

The combination of mechanical/chemical protocol was validated using a in vivo model in the oral cavity (Figure 5a), showing higher bacterial cell death (Figure 5b) than each therapy alone (~99% bacterial reduction;  $p < .05$ ). The Er:YAG laser application (alone or in combination with NaOCl) demonstrated greater cleaning potential with less adhered biofilm biomass on the surfaces ( $p < .05$ ; Figure 5c). Furthermore, a novel three-step decontamination protocol guarantees an effective in vivo cleaning potential, modulating periodontal complexes related to peri-implant diseases, such as red and orange microbial complexes (Figure 5d).

## 4 | DISCUSSION

This study was the pioneer to establish a three-step nonsurgical decontamination protocol for implant surfaces based on biofilm matrix

# Mechanical/chemical protocol

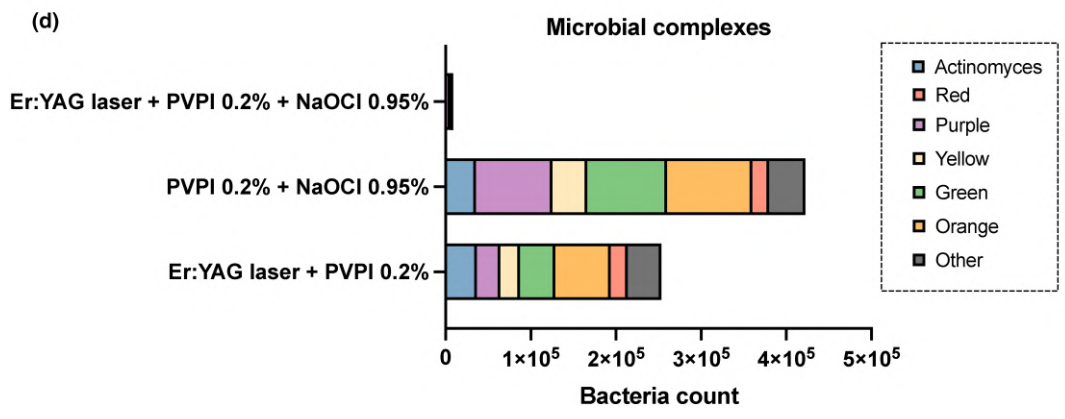
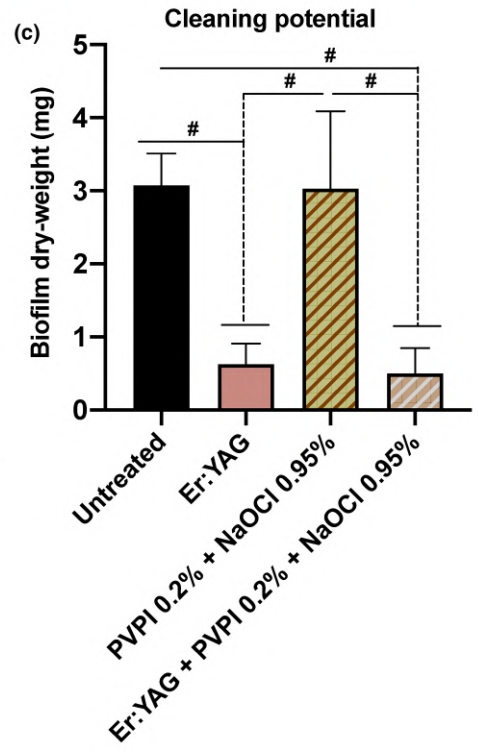
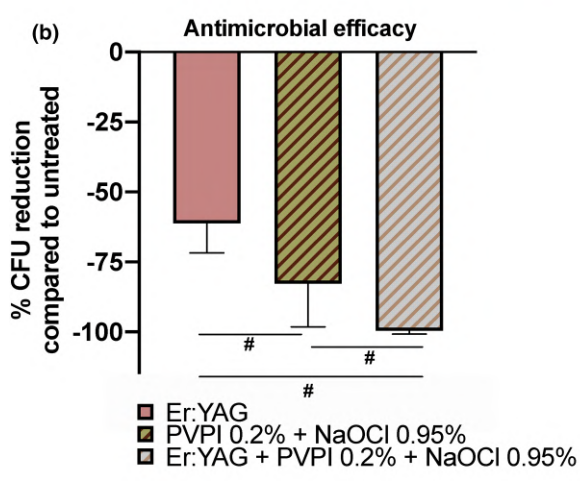
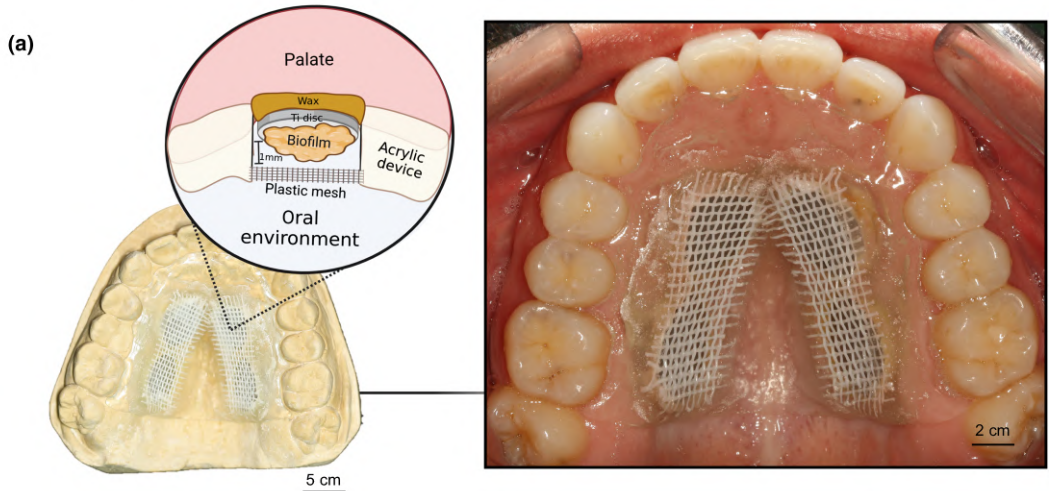


**FIGURE 5** In vivo antimicrobial effect of mechanical/chemical decontamination protocols. (a) Representative scheme of the palatal appliance used to form biofilms in the oral cavity. Figure created by Biorender (license number: YT24Y6OGOR). (b) % reduction of log-transformed viable colony-forming units (Log<sub>10</sub> CFU/mL) to check in situ antimicrobial efficacy and (c) biofilm-dry weight after mechanical/chemical (Er:YAG laser + PVPI 0.2% + NaOCl 0.95%) protocol ( $n=6$ ). (d) Bacterial load of periodontal complexes using the mean of total levels of the species evaluated by DNA-DNA checkerboard ( $n=4$ ). Data are expressed as the mean  $\pm$  standard deviation. Statistically significant differences between groups are indicated by symbols:  $\#p < .05$ , Tukey's HSD test.

disruption to enhance bacterial removal by antimicrobial and mechanical debridement and to evaluate possible surface damage. The biggest strength of this study was that we established a protocol for a 3D-printed Ti surface with a high surface roughness, which is the proof-of-concept for our biofilm matrix-degrading therapy. For the first time, we showed that the Er:YAG laser application led to minor morphological changes on Ti, with higher corrosion performance, effectively removing the biofilms and reducing recolonization, and favoring readhesion of gingival fibroblasts. After testing most of the commercially available chemical protocols currently used in the clinic, we also showed that the NaOCl 0.95% agent was able to drastically reduce the viability and metabolism of polymicrobial biofilms. Finally, we indicated a novel additional step to disrupt bacterial clustering and the exopolysaccharide matrix, creating a protocol that guarantees a surface almost free of live bacterial cells. Based on our findings, we defined a three-step protocol to remove biofilms from rough titanium implant surfaces as follows: Er:YAG laser [Step 1: to mechanically remove biofilms and possible calculus deposits]+PVPI 0.2% [Step 2: to disrupt biofilm matrix of any microbial clustering left behind on valleys of rough implant surfaces]+NaOCl 0.95% [Step 3: to eradicate remaining live bacteria] (Figure 6).

The rough titanium surfaces used in our study are fabricated through a novel 3D-printing technology. They have a unique and

complex micro- and macropography and geometry (Lee et al., 2021; Pingueiro et al., 2019), resulting in an ideal substrate to test effective decontamination protocols. Within our investigation, except for the water-air jet group, all other mechanical protocols tested altered the original surface patterns, although they were unable to significantly change the surface roughness and wettability. Regarding the Ti surface degradation, the rotating titanium brush promoted higher Ti particles, which can be explained by the simultaneous surface degradation and brush deterioration. Although the cause-effect relationship between Ti dissolution and peri-implant diseases is still not completely comprehended, Ti subproducts have been associated with an increased inflammatory response (Eger et al., 2018) and to stimulate putative pathogens grown on the Ti surface (Souza et al. 2020b). Moreover, Ti subproducts release can weaken the implant structure and increase the corrosion process (Costa, Abdo, et al., 2021). Importantly, the cumulative Ti subproducts released from the implant surface and brush (~0.4 ppm concentration) need further investigation to verify whether they could harm the peri-implant tissues and lead to further progression of peri-implantitis.

In addition to surface deterioration, mechanical instrumentation may remove the oxide film that is naturally formed on Ti-based implants, leading to oxidation and active attack on the material surface

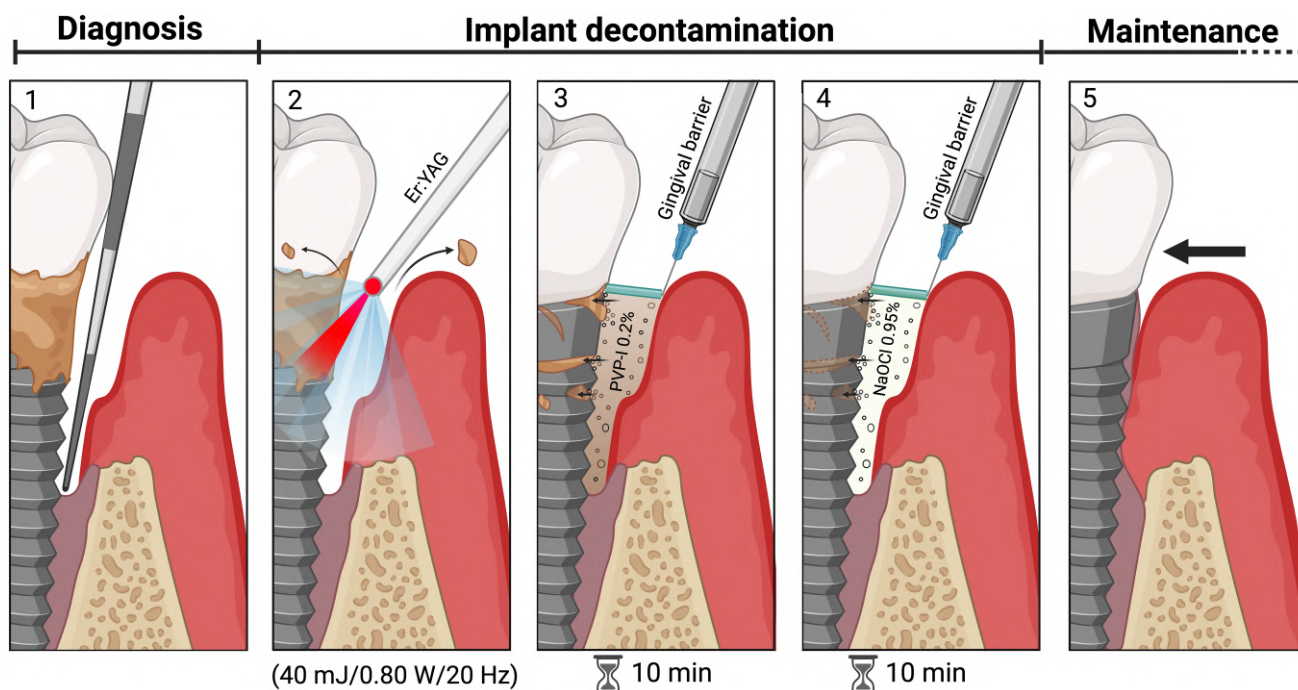


**FIGURE 6** Schematic representation of the possible three-step nonsurgical decontamination protocol for titanium-based dental implants. Figure created by Biorender (license number: YT24Y6OGOR).

(Costa, Nagay, et al., 2021). Er:YAG laser-treated surfaces displayed similar or slightly improved electric and electrochemical parameters compared with the as-received control. As we know, the characteristics of the TiO<sub>2</sub> film to be formed after laser irradiation are strongly dependent on the working parameters applied. Herein, the Er:YAG laser protocol with 40mJ, 0.80W, and 20Hz follows the manufacturer's recommendation for implant cleaning. We believe that the Er:YAG laser significantly reduces surface heterogeneities (smoothing), which are responsible for delaying the achievement of the equilibrium condition and behaving as a nonideal capacitor (Costa, Souza, Bertolini, et al., 2020; Costa, Souza, Cordeiro, et al., 2020). At the same time, the TiO<sub>2</sub> layer is probably thickened after laser irradiation and this hypothesis need to be further investigated. The residual energy from laser-assisted therapy can induce the formation of a duplex structure of the TiO<sub>2</sub> film with an inner compact high corrosion-resistant layer and an outer porous layer (AlMoharib et al., 2021). These modifications in the classic pattern of rough Ti surfaces likely induce a high homogeneity and compactness of the protective TiO<sub>2</sub> film, which can be associated with the best values in the electrical and electrochemical parameters found for this group. Thus, Er:YAG laser application seems to be a nondamaging decontamination method that improves the Ti oxide layer protective behavior without jeopardizing the Ti chemical composition. Regarding the cell readhesion onto treated surfaces after mechanical instrumentations, all groups resulted in low cytotoxicity and high metabolic activity of fibroblasts after 24h of culture. This finding can be associated with the direct preservation of the valleys region microstructure (Balderrama et al., 2020), which are the preferred cell adhesion sites on the surfaces, avoiding the peaks. This first phase determines the further behavior of the cells in contact with the implant surface (i.e., cell proliferation and differentiation), which could facilitate successful reosseointegration (Cao et al., 2018; Stein et al., 2023).

Mechanical debridement with hand currettes has been fronted as a preferred alternative in clinical practice (Figuro et al., 2014). Our findings do not fully support this recommendation, which indicates that titanium and Teflon currettes were ineffective in significantly reducing bacterial loads. A handful of studies (John et al., 2014; Luengo et al., 2022; Park et al., 2015; Sanz-Martín et al., 2021) have already demonstrated that the cleaning potential of rotatory titanium brushes outperformed hand currettes for several implant surfaces. Despite this superior cleaning performance, the irreversible surface damage and Ti release shown in this study make this a less attractive therapy. The present study shows that the water-air jet and Er:YAG laser groups successfully lowered microbial counts on implant surfaces without leading to surface deterioration. Notably, the water-air jet is ablative only and has no antimicrobial action, which, when used alone, leads to suboptimal clinical outcomes for sandblasted and etched implants (Al-Hashedi et al., 2017). In this study, Er:YAG laser-assisted therapy was advocated as a bactericidal strategy that causes bacterial vaporization and no implant surface damage and was the only treatment that promoted less bacterial recolonization and microbial profile modulation. The Er:YAG mechanism of action is related to the energy that

ruptures the cell membranes of bacteria when absorbed into intracellular water (AlMoharib et al., 2021), even at low energy densities (40mJ), as tested here.

Concerning the efficacy of the chemical agents, oxygenating products such as NaOCl 0.95% agent and HCOBc-based antiseptic were more effective for rough Ti surface disinfection than conventional antibiotics and chlorhexidine. NaOCl as a subgingival rinse for periodontitis has been proposed since the early 2000s for home care performed by patients as an effective, safe, and affordable periodontal antimicrobial therapy (Jorgensen et al., 2005; Slots, 2002, 2012). Since its mechanism of action is rather nonselective (oxidative burst), bacterial resistance toward NaOCl seems less likely than toward chemical agents, including antibiotics and chlorhexidine-based products. A recent clinical trial (Radulescu et al., 2022) demonstrated that a single topical application of NaOCl 0.95% in a gel form (Periosolv®) promotes a beneficial effect on clinical outcomes during supportive periodontal therapy. Multi-omics analysis of periodontal pocket microbial communities pre- and post-treatment with 0.25% sodium hypochlorite showed at baseline periodontal pathogens, such as *Porphyromonas*, *Treponema*, *Desulfovibrio*, and *Mycoplasma*, and after 2 weeks dramatic shifts in the most abundant taxa were observed, with only the genus *Desulfovibrio* remaining among the 20 most abundant taxa (Califf et al., 2017). Moreover, our study used PVPI 0.2% as a biofilm matrix-degrading therapy, which showed a synergistic antimicrobial effect with HCOBc and NaOCl, demonstrating that it as an emerging strategy with a high safety profile. Thus, an important finding in this study was that pre-treatment with PVPI made the greatest difference in the antimicrobial efficacy of NaOCl, which was shown to be even better than HCOBc-based antiseptic. These data suggest a possible synergistic effect when PVPI was used in combination with NaOCl, but the specific chemical reaction and mechanism of action for this synergism remain to be further explored.

To mimic the clinical conditions of biofilm formation over rough Ti surfaces, we employed an in situ model (Souza, Cury, et al., 2019) to develop oral biofilms inside subjects' mouths and validate the proposed mechanical/chemical protocol. With this model, we ascertained that Er:YAG laser+PVPI 0.2%+NaOCl 0.95% guarantees an effective action elimination of ~99% of oral biofilm formed over a rough Ti surface. Although the combination of PVPI+NaOCl was successful and could be continued by the patient as a home care measure on exposed rough implant surfaces, it is essential to remember that the Er:YAG laser as the first step is an important step for in-office decontamination because it helps to physically remove calculus deposits and biofilm.

Although we believe we developed a promising three-step biofilm removal technique for rough Ti surface decontamination without causing damage to the surface and altered cellular regrowth, we acknowledge some limitations in the present study. The presence of submucosal hard deposits (i.e., calculus) could not be simulated with the present design, which is a more challenging situation and another reason we suggested Er. YAG as the first step of the proposed decontamination protocol. Moreover, we consider that this optimized mechanical/chemical decontamination protocol needs to be further explored by clinical studies. Nevertheless, the combination

of Er:YAG laser + PVPI 0.2% + NaOCl 0.95% can be considered a reliable decontamination protocol for rough implant surfaces, providing enough biological plausibility and theoretical evidence for successful clinical translation and open new perspectives to improve non-surgical implant-related infection therapies.

#### AUTHOR CONTRIBUTIONS

RCC, TTST, JGSJ, and VARB contributed to conception and design, data acquisition, analysis, and interpretation, drafted and critically revised the manuscript. TTST, RCF, GP, CMS, KGSR, MF, and JAS contributed to design, data acquisition, drafted and critically revised the manuscript. All authors gave final approval and agreed to be accountable for all aspects of the work ensuring integrity and accuracy.

#### ACKNOWLEDGMENTS

This study was funded by The São Paulo Research Foundation (FAPESP), Grant/Award numbers: 2020/10436-4 to R.C.C., 2021/11753-6 to T.T.S.T., and 2020/05231-4 to V.A.R.B.; Conselho Nacional de Desenvolvimento Científico e Tecnológico (CNPq), Grant/Award number: #307471/2021-7 to V.A.R.B.; and Coordenação de Aperfeiçoamento de Pessoal de Nível Superior (CAPES), Finance code 001. The authors are indebted to Plenum® Company for supplying the samples used in this study. The authors also thank the Brazilian Nanotechnology National Laboratory (LNNano) at the Brazilian Center of Research in Energy and Materials (CNPEM) for the CLSM analysis facility and the Richard Landers for the XPS analysis facility. Finally, the authors express their gratitude to the volunteers for their valuable participation.

#### CONFLICT OF INTEREST STATEMENT

Jamil A. Shibli is currently the chief science officer at the M3 Health Ind. Com. de Prod. Med. Odont. e Correlatos S.A. (Plenum® Company; Jundiá, São Paulo, Brasil) and declares conflicts of interest. The other authors certify that they have no commercial or associative interest that represents a conflict of interest in the manuscript.

#### DATA AVAILABILITY STATEMENT

The data that support the findings of this study are available from the corresponding author upon reasonable request.

#### ORCID

Thais Terumi Sadamitsu Takeda  <https://orcid.org/0009-0004-7318-7133>

Martina Bertolini  <https://orcid.org/0000-0003-3619-6618>

Jamil A. Shibli  <https://orcid.org/0000-0003-1971-0195>

Valentim A. R. Barão  <https://orcid.org/0000-0002-6391-9917>

João Gabriel S. Souza  <https://orcid.org/0000-0001-5944-6953>

#### REFERENCES

- Al-Hashedi, A. A., Laurenti, M., Benhamou, V., & Tamimi, F. (2017). Decontamination of titanium implants using physical methods. *Clinical Oral Implants Research*, 28, 1013–1021.
- AlMoharib, H. S., Steffensen, B., Zoukhri, D., Finkelman, M., & Gyurko, R. (2021). Efficacy of an Er:YAG laser in the decontamination of dental implant surfaces: An in vitro study. *Journal of Periodontology*, 92, 1613–1621.
- Balderrama, Í., de F., Cardoso, M. V., Stuari, V. T., Oliveira, R. C., Matos, A. A., Greggi, S. L. A., & Sant'Ana, A. C. P. (2020). Residual decontamination chemical agents negatively affect adhesion and proliferation of osteoblast-like cells on implant surface. *International Journal of Implant Dentistry*, 6, 84.
- Berglundh, T., Armitage, G., Araujo, M. G., Avila-Ortiz, G., Blanco, J., Camargo, P. M., Chen, S., Cochran, D., Derks, J., Figuero, E., Hämmerle, C. H. F., Heitz-Mayfield, L. J. A., Huynh-Ba, G., Iacono, V., Koo, K.-T., Lambert, F., McCauley, L., Quirynen, M., Renvert, S., ... Zitzmann, N. (2018). Peri-implant diseases and conditions: Consensus report of workgroup 4 of the 2017 world workshop on the classification of periodontal and Peri-implant diseases and conditions. *Journal of Clinical Periodontology*, 45, S286–S291.
- Bowen, W. H., Burne, R. A., Wu, H., & Koo, H. (2018). Oral biofilms: Pathogens, matrix, and Polymicrobial interactions in microenvironments. *Trends in Microbiology*, 26, 229–242.
- Califf, K. J., Schwarzberg-Lipson, K., Garg, N., Gibbons, S. M., Caporaso, J. G., Slots, J., Cohen, C., Dorrestein, P. C., & Kelley, S. T. (2017). Multi-omics analysis of periodontal pocket microbial communities pre- and Posttreatment. *mSystems*, 2, e00016–e00017.
- Cao, J., Wang, T., Pu, Y., Tang, Z., & Meng, H. (2018). Influence on proliferation and adhesion of human gingival fibroblasts from different titanium surface decontamination treatments: An in vitro study. *Archives of Oral Biology*, 87, 204–210.
- Cosgarea, R., Rocuzzo, A., Jepsen, K., Sculean, A., Jepsen, S., & Salvi, G. E. (2022). Efficacy of mechanical/physical approaches for implant surface decontamination in nonsurgical submarginal instrumentation of peri-implantitis. A systematic review. *Journal of Clinical Periodontology*, 50(Suppl 26), 188–121.
- Costa, R. C., Abdo, V. L., Mendes, P. H. C., Mota-Veloso, I., Bertolini, M., Mathew, M. T., Barão, V. A. R., & Souza, J. G. S. (2021). Microbial corrosion in titanium-based dental implants: How tiny bacteria can create a big problem? *Journal of Bio- and Tribo-Corrosion*, 7, 136.
- Costa, R. C., Bertolini, M., Costa Oliveira, B. E., Nagay, B. E., Dini, C., Benso, B., Klein, M. I., Barão, V. A. R., & Souza, J. G. S. (2022). Polymicrobial biofilms related to dental implant diseases: Unravelling the critical role of extracellular biofilm matrix. *Critical Reviews in Microbiology*, 0, 1–21.
- Costa, R. C., Nagay, B. E., Bertolini, M., Costa-Oliveira, B. E., Sampaio, A. A., Retamal-Valdes, B., Shibli, J. A., Feres, M., Barão, V. A. R., & Souza, J. G. S. (2021). Fitting pieces into the puzzle: The impact of titanium-based dental implant surface modifications on bacterial accumulation and polymicrobial infections. *Advances in Colloid and Interface Science*, 298, 102551.
- Costa, R. C., Souza, J. G. S., Bertolini, M., Retamal-Valdes, B., Feres, M., & Barão, V. A. R. (2020). Extracellular biofilm matrix leads to microbial dysbiosis and reduces biofilm susceptibility to antimicrobials on titanium biomaterial: An in vitro and in situ study. *Clinical Oral Implants Research*, 31, 1173–1186.
- Costa, R. C., Souza, J. G. S., Cordeiro, J. M., Bertolini, M., de Avila, E. D., Landers, R., Rangel, E. C., Fortulan, C. A., Retamal-Valdes, B., da Cruz, N. C., Feres, M., & Barão, V. A. R. (2020). Synthesis of bioactive glass-based coating by plasma electrolytic oxidation: Untangling a new deposition pathway toward titanium implant surfaces. *Journal of Colloid and Interface Science*, 579, 680–698.
- Derks, J., & Tomasi, C. (2015). Peri-implant health and disease. A systematic review of current epidemiology. *Journal of Clinical Periodontology*, 42(Suppl 16), S158–S171.
- Eger, M., Hiram-Bab, S., Liron, T., Sterer, N., Carmi, Y., Kohavi, D., & Gabet, Y. (2018). Mechanism and prevention of titanium particle-induced inflammation and Osteolysis. *Frontiers in Immunology*, 9, 2963.
- Figuero, E., Graziani, F., Sanz, I., Herrera, D., & Sanz, M. (2014). management of peri-implant mucositis and peri-implantitis. *Periodontology 2000*, 66, 255–273.

- Heitz-Mayfield, L. J. A., & Mombelli, A. (2014). The therapy of peri-implantitis: A systematic review. *The International Journal of Oral & Maxillofacial Implants*, 29(Suppl), 325–345.
- Howe, M.-S., Keys, W., & Richards, D. (2019). Long-term (10-year) dental implant survival: A systematic review and sensitivity meta-analysis. *Journal of Dentistry*, 84, 9–21.
- Jervøe-Storm, P.-M., Hablützel, A. S., Bartels, P., Kraus, D., Jepsen, S., & Enkling, N. (2021). Comparison of irrigation protocols for the internal decontamination of dental implants—results of in vitro and in vivo studies. *Clinical Oral Implants Research*, 32, 1168–1175.
- John, G., Becker, J., & Schwarz, F. (2014). Rotating titanium brush for plaque removal from rough titanium surfaces – An in vitro study. *Clinical Oral Implants Research*, 25, 838–842.
- Jorgensen, M. G., Aalam, A., & Slots, J. (2005). Periodontal antimicrobials—Finding the right solutions. *International Dental Journal*, 55, 3–12.
- Lang, M. S., Ceruti, D. R., Miyamoto, T., & Nunn, M. E. (2016). Cell attachment following instrumentation with titanium and plastic instruments, diode laser, and titanium brush on titanium, titanium-zirconium, and zirconia surfaces. *The International Journal of Oral & Maxillofacial Implants*, 31, 799–806.
- Lee, C.-T., Huang, Y.-W., Zhu, L., & Weltman, R. (2017). Prevalences of peri-implantitis and peri-implant mucositis: Systematic review and meta-analysis. *Journal of Dentistry*, 62, 1–12.
- Lee, J., Lee, J.-B., Yun, J., Rhyu, I.-C., Lee, Y.-M., Lee, S.-M., Lee, M.-K., Kim, B., Kim, P., & Koo, K.-T. (2021). The impact of surface treatment in 3-dimensional printed implants for early osseointegration: A comparison study of three different surfaces. *Scientific Reports*, 11, 10453.
- Louropoulou, A., Slot, D. E., & Van der Weijden, F. (2014). The effects of mechanical instruments on contaminated titanium dental implant surfaces: A systematic review. *Clinical Oral Implants Research*, 25, 1149–1160.
- Luengo, F., Sanz-Esporrín, J., Noguerol, F., Sanz-Martín, I., Sanz-Sánchez, I., & Sanz, M. (2022). In vitro effect of different implant decontamination methods in three intraosseous defect configurations. *Clinical Oral Implants Research*, 33, 1087–1097.
- Ntrouka, V. I., Slot, D. E., Louropoulou, A., & Van der Weijden, F. (2011). The effect of chemotherapeutic agents on contaminated titanium surfaces: A systematic review. *Clinical Oral Implants Research*, 22, 681–690.
- Park, J.-B., Jeon, Y., & Ko, Y. (2015). Effects of titanium brush on machined and sand-blasted/acid-etched titanium disc using confocal microscopy and contact profilometry. *Clinical Oral Implants Research*, 26, 130–136.
- Pingueiro, J., Piattelli, A., Paiva, J., Figueiredo, L. C. de, Feres, M., Shibli, J., & Bueno-Silva, B. (2019). Additive manufacturing of titanium alloy could modify the pathogenic microbial profile: An in vitro study. *Brazilian Oral Research* 33: e065.
- Radulescu, V., Boariu, M. I., Rusu, D., Roman, A., Surlin, P., Voicu, A., Didilescu, A. C., Jentsch, H., Siciliano, V. I., Ramaglia, L., Vela, O., Kardaras, G., Sculean, A., & Stratul, S.-I. (2022). Clinical and microbiological effects of a single application of sodium hypochlorite gel during subgingival re-instrumentation: A triple-blind randomized placebo-controlled clinical trial. *Clinical Oral Investigations*, 26, 6639–6652.
- Renvert, S., Roos-Jansåker, A.-M., & Claffey, N. (2008). Non-surgical treatment of peri-implant mucositis and peri-implantitis: A literature review. *Journal of Clinical Periodontology*, 35, 305–315.
- Sakellari, D., Goodson, J. M., Kolokotronis, A., & Konstantinidis, A. (2000). Concentration of 3 tetracyclines in plasma, gingival crevice fluid and saliva. *Journal of Clinical Periodontology*, 27, 53–60.
- Sanz-Martín, I., Paeng, K., Park, H., Cha, J. K., Jung, U. W., & Sanz, M. (2021). Significance of implant design on the efficacy of different peri-implantitis decontamination protocols. *Clinical Oral Investigations*, 25, 3589–3597.
- Shibli, J. A., Ferrari, D. S., Siroma, R. S., de Figueiredo, L. C., de Faveri, M., Feres, M., Shibli, J. A., Ferrari, D. S., Siroma, R. S., de Figueiredo, L. C., de Faveri, M., & Feres, M. (2019). Microbiological and clinical effects of adjunctive systemic metronidazole and amoxicillin in the non-surgical treatment of peri-implantitis: 1 year follow-up. *Brazilian Oral Research*, 33, e080.
- Shibli, J. A., Rocha, T. F., Coelho, F., de Oliveira Capote, T. S., Saska, S., Melo, M. A., Pingueiro, J. M. S., de Faveri, M., & Bueno-Silva, B. (2021). Metabolic activity of hydro-carbon-oxo-borate on a multispecies subgingival periodontal biofilm: A short communication. *Clinical Oral Investigations*, 25, 5945–5953.
- Slots, J. (2002). Selection of antimicrobial agents in periodontal therapy. *Journal of Periodontal Research*, 37, 389–398.
- Slots, J. (2012). Low-cost periodontal therapy. *Periodontology*, 2000(60), 110–137.
- Souza, J. G. S., Cordeiro, J. M., Lima, C. V., & Barão, V. A. R. (2019). Citric acid reduces oral biofilm and influences the electrochemical behavior of titanium: An in situ and in vitro study. *Journal of Periodontology*, 90, 149–158.
- Souza, J. G. S., Costa Oliveira, B. E., Bertolini, M., Lima, C. V., Retamal-Valdes, B., de Faveri, M., Feres, M., & Barão, V. A. R. (2020). Titanium particles and ions favor dysbiosis in oral biofilms. *Journal of Periodontal Research*, 55, 258–266.
- Souza, J. G. S., Costa Oliveira, B. E., Costa, R. C., Bechara, K., Cardoso-Filho, O., Benso, B., Shibli, J. A., Bertolini, M., & Barão, V. A. R. (2022). Bacterial-derived extracellular polysaccharides reduce antimicrobial susceptibility on biotic and abiotic surfaces. *Archives of Oral Biology*, 142, 105521.
- Souza, J. G. S., Cury, J. A., Ricomini Filho, A. P., Feres, M., de Faveri, M., & Barão, V. A. R. (2019). Effect of sucrose on biofilm formed in situ on titanium material. *Journal of Periodontology*, 90, 141–148.
- Souza, J. G. S., Lima, C. V., Costa Oliveira, B. E., Ricomini-Filho, A. P., Faveri, M., Sukotjo, C., Feres, M., Del Bel Cury, A. A., & Barão, V. A. R. (2018). Dose-response effect of chlorhexidine on a multispecies oral biofilm formed on pure titanium and on a titanium-zirconium alloy. *Biofouling*, 34, 1175–1184.
- Stein, J. M., Conrads, G., Abdelbary, M. M. H., Yekta-Michael, S. S., Buttler, P., Glock, J., Sadvandi, G., Kaufmann, R., & Apel, C. (2023). Antimicrobial efficiency and cytocompatibility of different decontamination methods on titanium and zirconium surfaces. *Clinical Oral Implants Research*, 34(1), 20–32.
- Tenenbaum, H., Jehl, F., Gallion, C., & Dahan, M. (1997). Amoxicillin and clavulanic acid concentrations in gingival crevicular fluid. *Journal of Clinical Periodontology*, 24, 804–807.
- Yang, T., Xie, L., Hu, X., He, K., Zhu, Z., Fan, L., & Tian, W. (2023). Residual extracellular polymeric substances (EPS) detected by fluorescence microscopy on dental implants after different decontamination. *Materials Chemistry and Physics*, 296, 127242.

## SUPPORTING INFORMATION

Additional supporting information can be found online in the Supporting Information section at the end of this article.

**How to cite this article:** Costa, R. C., Takeda, T. T. S., Dini, C., Bertolini, M., Ferreira, R. C., Pereira, G., Sacramento, C. M., Ruiz, K. G. S., Feres, M., Shibli, J. A., Barão, V. A. R., & Souza, J. G. S. (2023). Efficacy of a novel three-step decontamination protocol for titanium-based dental implants: An in vitro and in vivo study. *Clinical Oral Implants Research*, 00, 1–14. <https://doi.org/10.1111/clr.14224>